Turbulent Mixing and Atomization in a Confined Shear Layer

R. C. Prior Jr.,* K. V. Tallio,† and A. M. Mellor‡
Vanderbilt University, Nashville, Tennessee 37235

The influence of mean air velocity and shear-layer strength on turbulent mixing times and airblast atomization is investigated. Experiments carried out in a two-dimensional, two-stream wind tunnel have been developed to simulate the mixing region (i.e., shear layer with liquid injection) found in the primary zone of a gas turbine combustor. A turbulent mixing time defined as the ratio of length scale and fluctuating component of velocity (ℓ/u_{rms}) is found to be an appropriate parameter to describe the mixing process. For a given value of shear-layer strength, these mixing times are found to be inversely proportional to the inlet mass average velocity. These mixing times are also shown to decrease with increasing shear-layer strength. Thus both shear-layer strength and inlet velocity have a strong influence on mixing time and, in relation to an actual combustor, on flame stabilization and combustion efficiency. Both of these parameters are also found to influence atomization quality, with Sauter mean diameter increasing with increasing shear-layer strength and decreasing with increasing velocity.

Nomenclature

a = empirical constant
A_a = cross-sectional area at injector tip
d_{comb} = combustor diameter or annulus height
d_{32} = Sauter mean diameter
D = internal dimension of square test section, = 76.2 mm
D_p = injector characteristic dimension, = 152.4 mm
I/I_0 = transmitted intensity in forward-scattering spray measurement
ℓ = integral axial length scale
ℓ_{co} = combustor length scale for CO emissions
ℓ_{pri} = distance from fuel injector tip to centerline of combustor primary holes
ℓ_{sec} = distance from fuel injector tip to centerline of combustor secondary holes
R = correlation coefficient for least squares fit
t = thickness of atomizer upstream of prefilming ramp
u_{rms} = root mean square axial velocity
U_A = mass average air velocity in Eq. (1), = $W_a/\rho_a A_a$
U_{AAS} = mass average air velocity on air only side of splitter plate
U_{AFS} = mass average air velocity on fuel injection side of splitter plate
$U_{\max}$ = maximum axial velocity at indicated position
U_x = local axial velocity at indicated position
W_a = air mass flow rate
W_ℓ = liquid mass flow rate
X = axial flow coordinate
Y = transverse flow coordinate
Z = third Cartesian flow coordinate
λ = shear-layer strength, = $(U_{AFS} - U_{AAS})/(U_{AFS} + U_{AAS})$
μ_ℓ = liquid viscosity
ρ_a = air density
ρ_ℓ = liquid density
σ_ℓ = liquid surface tension
τ_{eb} = evaporation time for droplet of Sauter mean diameter
τ_{hc} = ignition delay time for fuel vapor/air mixture
$\tau_{s\ell,co}$ = mixing time, evaluated in terms of combustor geometry and mean velocity, near origin of shear layer surrounding primary zone recirculating flow
$\tau_{s\ell,\text{global}}$ = definition of mixing time for test tunnel, analogous to $\tau_{s\ell,co}$ for a turbine combustor
$\tau_{s\ell xy}$ = local eddy lifetime, defined as integral length scale divided by *rms* velocity at measurement location (X/D, Y/D, Z/D = 0)
$\tau_{s\ell,x0}$ = local eddy lifetime measured as function of X/D on geometric centerline of test section (X/D, Y/D = Z/D = 0)
$\tau_{s\ell,00}$ = local eddy lifetime measured at origin of shear layer (X/D = 0.03, Y/D = Z/D = 0)
ϕ = nozzle efficiency factor

Introduction

FLAME holding in high-velocity flows requires introduction of recirculation zones that produce residence times sufficiently long for liquid fuel evaporation, fuel vapor/air mixing, and ignition. Around these regions of recirculation, shear layers exist that in the case of gas turbine combustion are thought to be responsible for determining the flame stabilization limit,[1,2] CO emissions,[3,4] and combustion efficiency.[5]

Estimates of these time requirements in terms of combustor inlet conditions and geometry and fuel and injector properties can be used in a quantitative fashion to correlate measurements from both laboratory and engine burners. For example, for lean blowoff in liquid-fueled systems, characteristic times associated with the evaporation of a drop of mean diameter in the spray (τ_{eb}), fuel vapor/air ignition delay time in the shear layer (τ_{hc}), and the average (igniting) turbulent eddy lifetime ($\tau_{s\ell,co}$) can be evaluated. Simple considerations suggest that a stable flame will occur only if $\tau_{s\ell,co} \geq \tau_{hc} + a\tau_{eb}$; that is, if the shear-layer residence time is sufficient to equal or exceed the sum of evaporation and ignition delay times.

This limit equation can be calibrated against engine data to yield values of slope and constant a.[6,7,8] Figure 1 shows the limit equation as the solid line, based on measured fuel/air ratios at blowoff for three widely differing gas turbine combustors (T63, AGT1500, and J85). The various symbols represent measured blowoff occurrences for the combustors and

Received July 15, 1989; revision received June 6, 1990; accepted for publication Sept. 21, 1990.

*Graduate Assistant, Department of Mechanical Engineering; currently Power Staff Engineer, Power Technology Department, International Paper Company.

†Graduate Assistant, Department of Mechanical Engineering; currently Research Engineer, Engine Research Department, Ford Motor Company. Member AIAA.

‡Centennial Professor of Mechanical Engineering. Member AIAA.

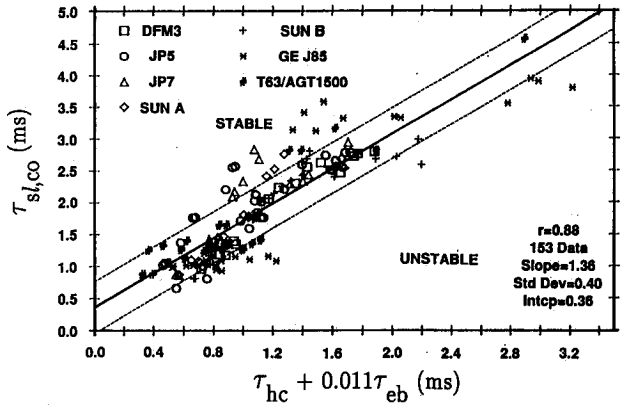

Fig. 1 J85, T63, and AGT1500 lean blowoff correlation for gas turbine combustors[8] (all data for J85 except those designated T63/AGT1500).

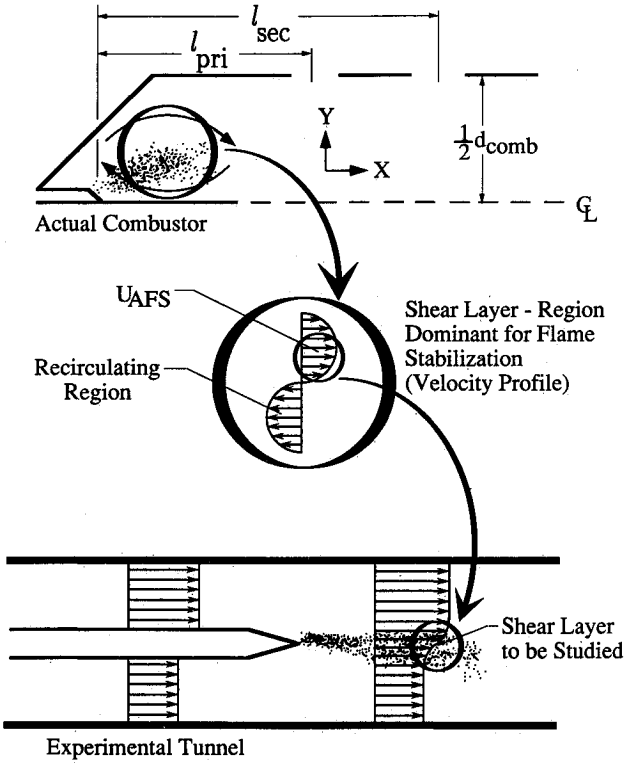

Fig. 2 Comparison of the primary zone of an actual combustor with the experimental configuration.

test fuels, and according to the above criterion, stable flames result only above the solid line. See Jarymowycz and Mellor[7] for evaluation of τ_{eb} and τ_{hc}; $\tau_{st,co}$ is discussed below.

The focus of the present work is, first, why such a simple model works, and, second, what is the source of the scatter exhibited by the data in Fig. 1. For example, empirical correlations[9] for Sauter mean diameter (d_{32}) must be used with caution, particularly when extrapolated to the high-pressure and temperature recirculating zones associated with gas turbine combustor primary zones. Based on the d^2 law of droplet evaporation[10] modified for forced convection,[11,12] τ_{eb} will reflect this inaccuracy as well as that associated with the use of integral scattering measurements for d_{32}.[13] Tuttle et al.[14] surmised that $\tau_{st,co}$ evaluated as a characteristic flameholder dimension divided by the flow velocity at the flameholder station (i.e., the origin of the shear layer) is directly proportional to the lifetime of a mean eddy, that is, the turbulent length scale divided by the *rms* velocity $\tau_{st,xy}$ in that region of the flow. To study this in detail, a nonreacting two-dimensional shear flow that simulates the primary zone of a gas turbine combustor (Fig. 2) is developed with known geometry (characteristic flameholder dimension) and adjustable inlet conditions. The ratio of this dimension to the inlet velocity can be compared with the ratio of experimentally determined length scale and u_{rms} obtained at the shear-layer origin. It is then possible to determine whether these two ratios are in fact proportional.

Experimental

The apparatus selected for the study is shown schematically in Fig. 3 and employs a vertically down-flowing wind tunnel of square cross section with internal dimension D = 76.2 mm. A Reliance Model 608 blower followed by a Chromalox Model GCH-45175 heater feeds the air to both sides of the tunnel in which the splitter plate terminates in a two-dimensional prefilming airblast injector designed following Rizk and Lefebvre.[15] Suitable valving shown in Fig. 3 allows differing air velocities to be chosen for the two sides of the splitter plate.

Figure 3 also shows the liquid system that via the splitter plate feeds a manifold under a porous plate as shown in Fig. 4. For the tests reported here, water was the only liquid employed, and its temperature and pressure in the manifold were nominally 35–50°C and 1.35 atm. Flow rate was measured with a Brooks Model 1110-08H2GIR flowmeter and maintained by means of a Teel Model 1P777 pump.

Also shown in Fig. 4 is the coordinate axis of the test rig. Variation in the axial distance X was obtained by translation

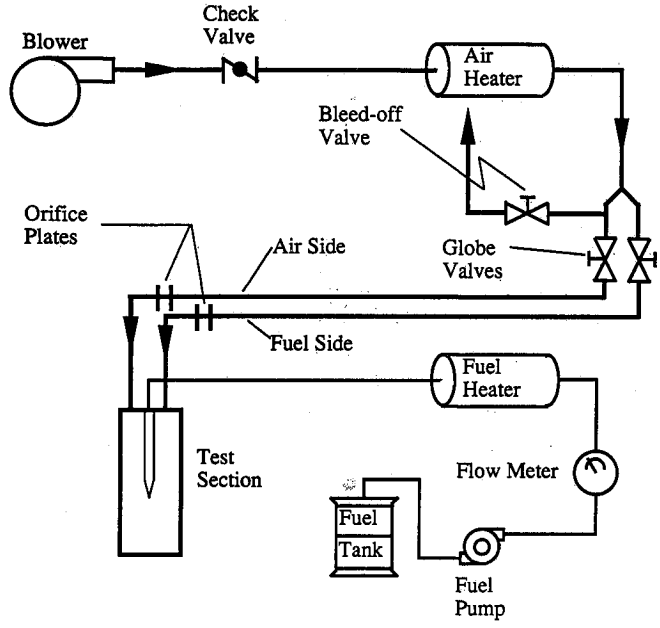

Fig. 3 Schematic of test facility.

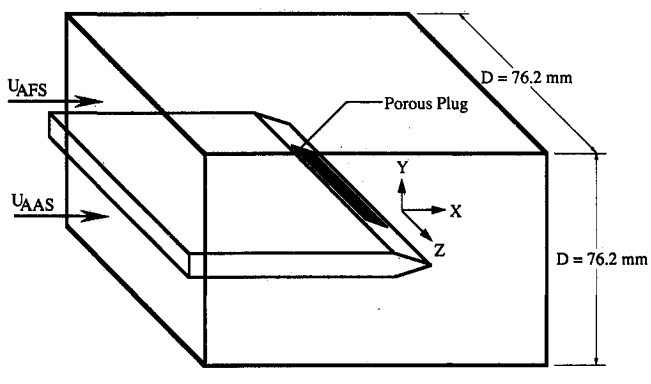

Fig. 4 Tunnel test section and coordinate system.

of the splitter plate-liquid nozzle upstream of the measurement station in the test section. Y is the direction in which the shear layer grows for shear flows, and Z measurements reveal the two-dimensionality of the flow. The thickness of the splitter plate is 1.03 cm, and the included angle at its tip is 15 deg.

Hot-film anemometry (TSI Model IFA-100) provided values of mean velocity, *rms* velocity, and turbulent length scale (through autocorrelations and Taylor's hypothesis), in the absence of droplets. No hot-wire measurements were performed in regions where significant numbers of drops were present. Forward-scattering and laser extinction measurements using an optical apparatus similar to that of Rizk and Lefebvre[15] provided Sauter mean diameter and liquid volume concentration. Tallio et al.[16] provide further details of test apparatus and instrumentation, as well as data in addition to those reported here.

Results and Discussion

Preliminary measurements were conducted to study the gas phase flow in the tunnel, without liquid injection, and performance of the prefilming airblast nozzle. These results will be reviewed first, followed by a presentation of the more detailed studies.

Preliminary Measurements

In the preliminary test matrix shown in Table 1, for experiments without liquid injection the intent was to compare results with other shear-layer studies, both confined and unconfined. Here U_{AFS} is the air mass average velocity on the porous plate side of the injector, where the liquid is introduced (see Fig. 4), λ is a shear-layer strength parameter, defined as the difference in the air velocities divided by their sum, and U_{AAS} is the air mass average velocity on the air-only side of the injector. Values of U_{AFS} in cases 1, 7, and 8 were chosen from velocity conditions used by Rizk and Lefebvre[15] with equal air velocities ($\lambda = 0$). Then λ was varied from 0 to 1 at constant U_{AFS} to determine the effect of shear-layer strength (cases 1, 2, 3, and 5), and the final cases 4 and 6 gave variations in U_{AFS} at constant λ. Air temperature for all cases was nominally 115°C at an absolute pressure of 1.1–1.2 atm, both monitored at the ASME-standard orifice plate locations noted in Fig. 3, approximately 3.0 m upstream of the test section.

Gas Phase

Y and Z profiles (probe traverses in the direction perpendicular and parallel to the plane of the atomizer, respectively) at $X/D = 0.03$, 1.00, and 2.00 were obtained for both mean and *rms* axial velocities in all eight cases shown in Table 1. Only those Y and Z mean velocity profiles that when integrated across the tunnel cross section gave within 5% of the orifice-plates-measured total mass flow were considered acceptable, except for case 3 in which the anticipated flow recirculation was observed. Three-dimensional flow effects were found only for case 2 (with $\lambda = 0.67$) at $X/D = 2.0$. Figure 5 shows Y profiles of axial velocity at $X/D = 0.03$ for case 4; the splitter plate and wall boundary layers at $Y/D = \pm 0.5$ and the peak turbulent intensities associated with these regions are exhibited clearly. The shear layer develops at larger values of X/D, the actual value depending on the magnitudes of U_{AFS} and λ (see Marakovits[17]).

Table 1 Preliminary test matrix

Case	U_{AFS}, m/s	λ	U_{AAS}, m/s
1	73.9	0.0	73.9
2	73.9	0.67	14.6
3	73.9	1.0	0.0
4	42.5	0.33	21.4
5	73.9	0.33	37.2
6	100.4	0.33	50.6
7	42.5	0.0	42.5
8	100.4	0.0	100.4

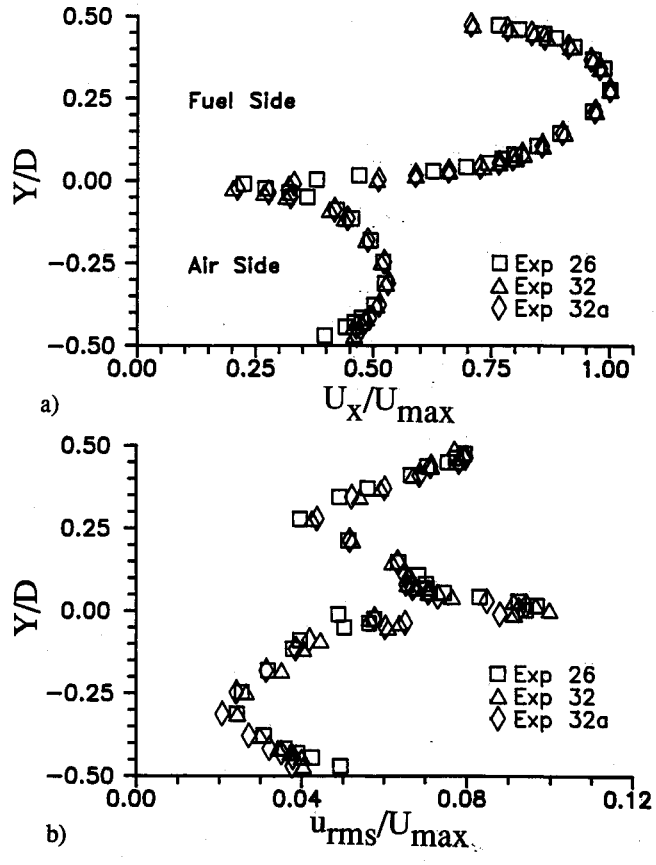

Fig. 5 *Y* profiles of normalized a) mean and b) *rms* velocities at $X/D = 0.03$ and $Z/D = 0.0$ (case 4 without water injection); U_{max} for experiment 26 = 55.51 m/s, for experiment 32 = 53.09 m/s, and for experiment 32a = 54.05 m/s.

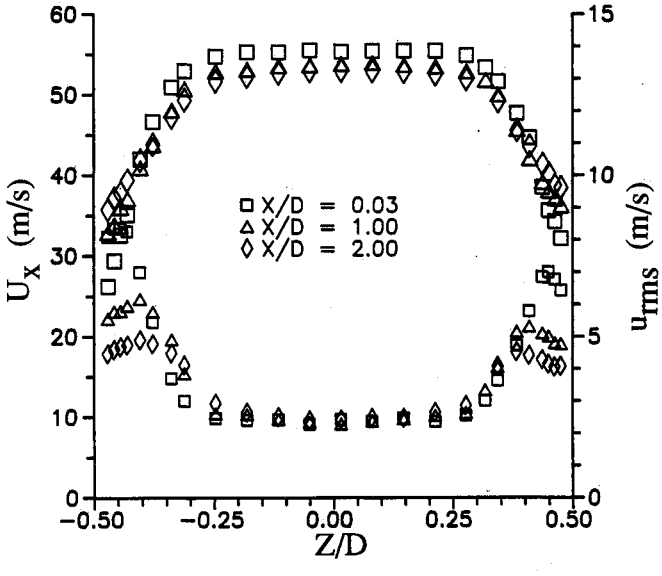

Fig. 6 *Z* profiles of mean (large symbols) and *rms* (small symbols) velocities at $Y/D = 0.25$ (case 7 without water injection).

Z profiles were also used to establish if uniform flow exists over the width of the porous plug shown in Fig. 4 (50 mm, or Z/D from −0.3 to +0.3). Experimental results showed that for all cases of the preliminary matrix, except for the second and third, the Z profiles were flat in this region. Figure 6 shows these data for case 7 at $Y/D = 0.25$ (on the liquid injection side of the nozzle). Both mean and *rms* axial ve-

locities are shown for all axial distances studied, and all profiles are two-dimensional for the required Z distance.

The shear-layer momentum[18] and vorticity thicknesses[19] were investigated to compare with other studies. These will grow nonlinearly with axial distance until the flow becomes fully developed and then will grow linearly. In the present work[17] these values were only evaluated at axial distances of X/D = 1.0 and 2.0 and found to be of similar magnitude to those reported in the literature. For the cases where $\lambda = 0.33$, equal values of momentum or vorticity thickness independent of U_{AFS} indicated a constant shear-layer width. The additional axial and upstream boundary-layer thickness measurements required to characterize the flow fully and to compare with other studies were not performed for these exploratory results.

Liquid Phase

Mean droplet size (d_{32}) and transmission measurements were conducted for selected cases from X/D = 0.50–2.00 in one-half-tunnel-diameter increments for those cases where spray impingement on the Y walls did not restrict optical access (generally $\lambda < 0.33$). At each downstream location, both optical measurements were attempted at the centerline locations (Z/D = 0.00) and at 5 mm (0.066 D) increments on either side of the centerline, for a total of five measuring locations. In the direction parallel to the spray sheet, optical measurements were precluded by droplet impingement that occurred on the Z walls at X/D less than 0.5.

The time average two-dimensionality of the spray from the nozzle is demonstrated in Fig. 7, where integral d_{32} and transmitted intensity, both measured with the optical path parallel to the Y axis, are presented as functions of Z/D for two liquid flow rates. Three d_{32} measurements were obtained at each value of Z/D for each flow rate. The d_{32} data exhibit scatter of ±3 μm for W_ℓ = 16.6 g/s and ±6 μm for W_ℓ = 9.5 g/s, typical of results at all X locations studied for this case and others. Variation in mean drop size across the spray is ±5 μm for both flow rates, indicating uniformity of spray d_{32} as the data are within the limits of scatter observed by others using this measurement technique.[20] The slight increase in transmission at the positive Z locations can be attributed to a lower liquid flow rate through the corresponding portion of the porous plate due to blockage and/or marring of the porous surface. Since care was taken to ensure that the Z wall boundary layers do not penetrate to the Z edges of the porous plate (see Fig. 6), the measurements of Fig. 7, which are restricted to approximately the center half of the plate, are considered satisfactory.

Also apparent is that the d_{32} is not a function of liquid flow rate, a consequence of the low liquid-to-air ratios used in this study (maximum of 0.05). Lefebvre[9] observed this phenomenon in other prefilming airblast atomizers for liquid-to-air ratios below 0.2.

Atomization measurements for d_{32} made at Z/D = 0 have been compared to those of Rizk[21] for a similar flat prefilming airblast atomizer and are shown in Fig. 8 (some of these measurements were obtained at air velocities and shear-layer strengths other than the velocities listed in the preliminary test matrix). An X/D = 1.83 was chosen to correspond to the axial location used by Rizk, who used a shroud at the atomizer tip to decrease the cross-sectional area. The flow from this rig was unconfined (at ambient room conditions) downstream of the atomizer tip. Two values of plate porosity were evaluated with water in the present study, while Rizk examined two different fluids.

Sauter mean diameters were calculated from Lefebvre's[9] equation for axisymmetric and flat prefilming atomizers in terms of air and liquid flowrates and properties:

$$d_{32} = \frac{1}{\phi}\left(1 + \frac{W_\ell}{W_a}\right)\left[0.073\left(\frac{\sigma_\ell}{\rho_a U_A^2}\right)^{0.6}\left(\frac{\rho_\ell}{\rho_a}\right)^{0.1} D_p^{0.4} + 0.015\left(\frac{\mu_\ell^2 D_p}{\sigma_\ell \rho_\ell}\right)^{0.5}\right] \quad (1)$$

where U_A is taken as U_{AFS} for the present data. Lefebvre[9] introduced a nozzle efficiency factor (ϕ) and characteristic dimension D_p as well, so that geometrically dissimilar designs can be compared directly; for flat prefilmers, D_p is set equal to twice the width of the atomizer. For ϕ he uses values between 0.6 and 1.0 to relate several differing injectors. The

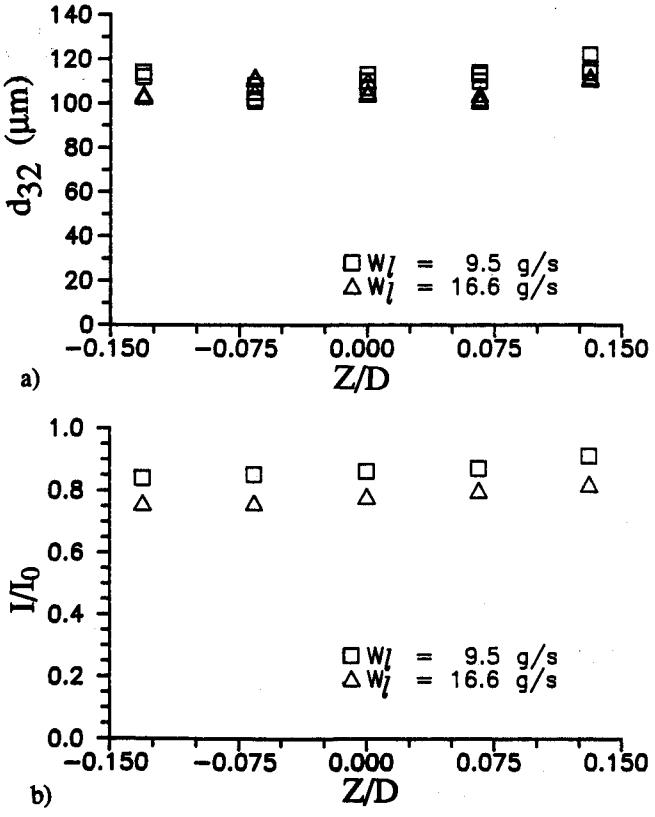

Fig. 7 Z profiles of a) Sauter mean diameter and b) transmitted intensity for case 8 at X/D = 2.0.

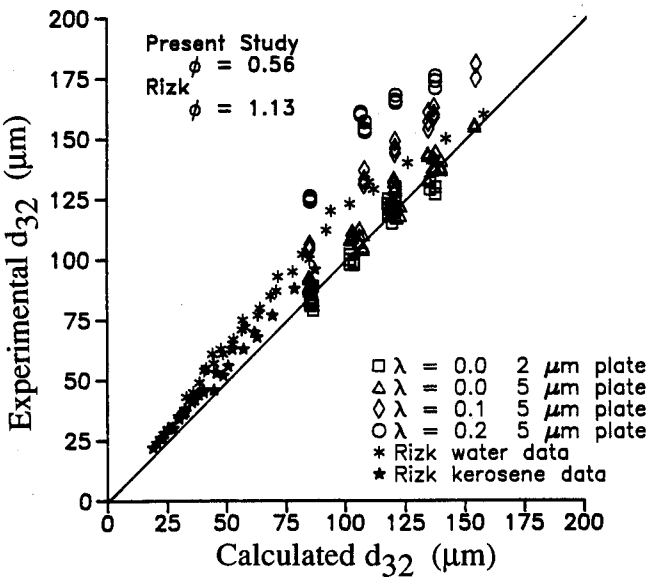

Fig. 8 Measured vs calculated Sauter mean diameters at X/D = 1.83 using Lefebvre's Eq. (1).

present data for $\lambda = 0$ in Fig. 8 were correlated with an efficiency factor of 0.563 for the geometry as shown in Fig. 4 and 1.13 for the measurements of Rizk. Lefebvre[9] attributes variations in efficiency factor to modifications in injector design, and such exist between the present atomizer and Rizk's[21]: as noted, the latter employs a shroud at the atomizer tip, eliminated here to minimize recirculation and simplify the flowfield for numerical analysis. The deviations remaining between Rizk's water and kerosene data in Fig. 8 are indicative of the difficulty in using empirical correlations to estimate changes in d_{32} (and thus τ_{eb}) when liquid properties are varied.

Accurate correlations for d_{32} are necessary to limit scatter in droplet lifetime calculations for the characteristic time models. From Fig. 8, liquid properties are not correlated to better than 10%, while changes in atomizer geometry can produce differences of 50% or more, as evidenced by the wide range of efficiency factors required for the above correlation. Since errors in predicted Sauter mean diameter can create discrepancies in τ_{eb} of order $d_{32}^{2.0}$ (but depend on the convective correlation chosen[11,12]), it is apparent that they can cause a significant amount of scatter on the ordinate of Fig. 1. For example, a 33% error at 100 μm (taking Jet-A fuel in a 750 K environment with 30 m/s relative velocity) can move a given datum point in Fig. 1 ± 0.43 ms, or ± 1 standard deviation. Thus one improvement in the model's predictive ability for τ_{eb} requires more accurate correlations for or actual in situ measurements of d_{32}.

An additional parameter not considered in correlation equations, but which warrants investigation, is the shear-layer strength. To study in detail its effect on d_{32}, additional cases were added to the preliminary matrix to provide a broader range of U_{AFS}. As shown in both Figs. 8 and 9, d_{32} increases with an increase in λ for constant U_{AFS}. At a given value of U_{AFS}, an increase in d_{32} of as much as 33%, or 40 μm, is observed due solely to increasing shear-layer strength from $\lambda = 0$ to 0.2. These results are consistent with the findings of other researchers[22] and are due to momentum transfer from the high-velocity airstream deflecting the liquid sheet to the low-velocity side, resulting in a reduction of effective atomizing air velocity and thereby increasing mean drop size.

Also consistent with data of other researchers is the effect of U_{AFS} on d_{32} in Fig. 9. At constant λ, d_{32} decreases with increasing values of U_{AFS} because of the additional momentum transfer to the liquid sheet. For zero shear-layer strength, the experimental data show a 37% decrease in average d_{32} (141 to 97 μm) corresponding to an increase in U_{AFS} from 82.6 to 122.0 m/s. Over the same velocity range, the correlation equation predicts a 37% decrease in d_{32}. Similar decreases in experimental d_{32} are observed for $\lambda = 0.1$ and 0.2 (35 and 31%, respectively).

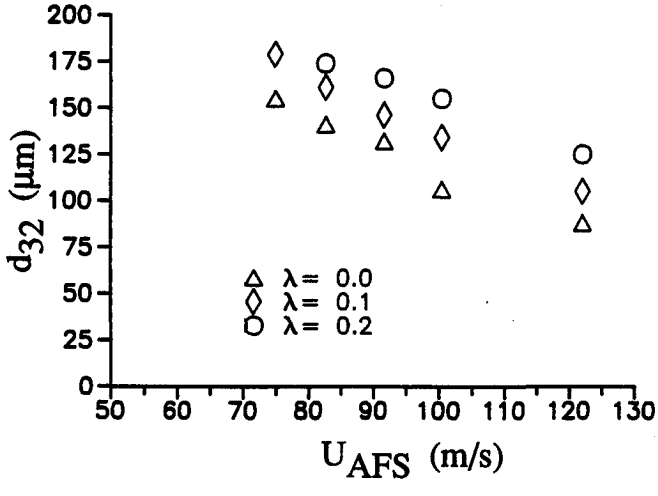

Fig. 9 Average Sauter mean diameter vs U_{AFS} for various shear-layer strengths at $X/D = 1.83$ (5 m porous plate).

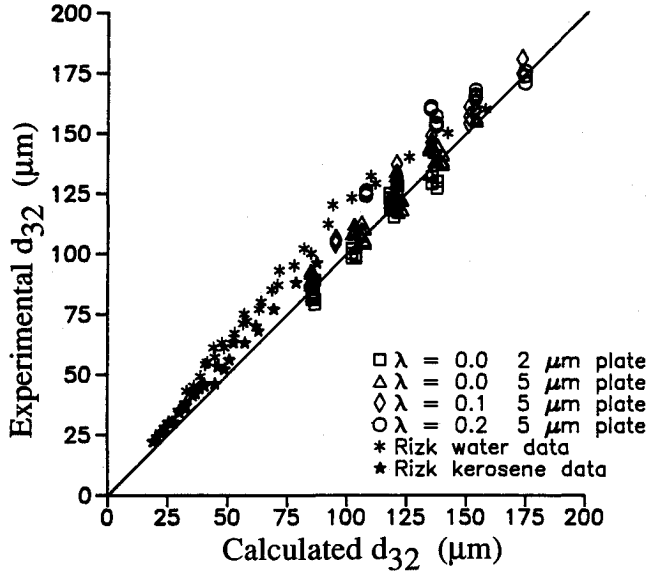

Fig. 10 Measured vs calculated Sauter mean diameters at $X/D = 1.83$ using Lefebvre's equation modified to include shear-layer strength.

If U_A in Eq. (1) is replaced with average velocity,

$$\frac{1}{2}(U_{AFS} + U_{AAS}) = U_{AFS}/(1 + \lambda) \tag{2}$$

then data for $\lambda > 0$ can be collapsed to Lefebvre's correlation, as shown in Fig. 10. The average velocity in cases with shear layer emanating from the prefilmer tip is identical to the mass-average velocity from continuity. Thus, as shear-layer strength increases (at constant U_{AFS}), the decrease in average velocity leads to a deterioration in overall atomization (e.g., d_{32}) observed in the present investigation and that of Sattelmayer and Wittig.[22]

The opposite case, with $U_{AFS} < U_{AAS}$ and $\lambda < 0$, was not studied in the present work. Sattelmayer and Wittig performed limited experiments for this case but decreased U_{AFS} correspondingly to maintain a constant value of average velocity, as defined by the left-hand side of Eq. (2). They found atomization deteriorated, in contrast to the prediction of Eq. (2), and attributed these results to a nonoptimum interaction between average shear stress and waves formed in the liquid film.

The experimental work discussed above was undertaken to characterize the gas-phase flow in the test tunnel and to relate atomizer performance insofar as possible to other two-dimensional and axisymmetric prefilming airblast atomizers. This work also established a set of baseline operating conditions for further investigation of the mixing time $\tau_{st,co}$.

Detailed Measurements

The final test matrix, shown in Table 2, was chosen based on several criteria and constraints. It was desirable to repeat some cases of the preliminary test matrix to ascertain if flow conditions within the test section could be reproduced accurately. Accordingly, the final test matrix includes cases 1, 7, and 8 of the preliminary test matrix. Second, it was necessary to eliminate cases that involved three-dimensional or recirculating flow, which limited λ to less than 0.67 (another consistent constraint mentioned earlier was that $\lambda = 0.33$ or greater resulted in spray impingement on the Y windows, making accurate droplet sizing measurements impossible). Thus, the final values of shear-layer strength selected were between 0.0 and 0.2.

Table 2 Final test matrix

Case	U_{AFS}, m/s	λ	U_{AAS}, m/s
1	73.9	0.0	73.9
7	42.5	0.0	42.5
8	100.4	0.0	100.4
10	82.6	0.0	82.6
11	82.6	0.1	67.1
12	82.6	0.2	54.2
13	100.4	0.2	63.4
14	73.9	0.2	46.1

For all eight cases of the final test matrix, Y profiles of length scale and *rms* and mean velocity at the inlet station ($X/D = 0.03$) were obtained at $Z/D = 0.0$. In addition, two cases were chosen to study the evolution of mean and *rms* velocities and length scales in detail and to compare with calculations from a parabolic, two-dimensionsal code using the k-ϵ turbulence model.[23] Case 1 is a repeated case from the preliminary test matrix and so can be compared with preliminary test matrix results. Case 14 was selected for study for two reasons: to determine mixing times with a strong shear layer and to maintain the same fuel side velocity as in case 1, making comparisons between cases 1 and 14 possible. The detailed flow measurements are reported further in Refs. 16 and 23.

Flowfield measurements were obtained 0.66 tunnel diameters upstream of the origin ($X/D = -0.66$) to observe the flow directly before the atomizer ramp. Measurements obtained at 0.33 tunnel diameters upstream revealed flow characteristics part way through the flow expansion due to the decreasing thickness of the ramp. Mean and *rms* velocity and length scale measurements taken at 0.03 tunnel diameters downstream of the atomizer tip enabled the geometric origin of the shear layer to be observed and provided data for the calculation of initial mixing times. Further downstream of the atomizer gas phase measurements were taken to observe the shear-layer growth as the flow progressed and to obtain downstream mixing times for comparison with the mixing time at the shear-layer origin.

Velocity measurements at each axial location involved three Y profiles and three Z profiles. Y profiles were located at the centerline ($Z/D = 0.00$) and at one-quarter tunnel diameter on either side of the centerline ($Z/D = \pm 0.25$). Likewise, Z profiles were located at $Y/D = 0.00$ and ± 0.25. As before, integrated mass flow rates were within 5% of those measured with the orifice plates.

Figures 11a and 11b compare Y profiles of mean and *rms* velocity data from case 1 of both the preliminary and final test matrices. Z-averaged mean or *rms* velocity profiles are reported for case 1 of the final test matrix whereas velocity profiles from case 1 of the preliminary test matrix are centerline ($Z/D = 0.00$) values.

The mean velocity profiles shown here (and downstream profiles not shown) show good agreement except in the boundary layers near the outer walls approaching $Y/D = \pm 0.50$. The measurements for the present work demonstrate freestream and wake velocity variations of less than 7% along the Z axis, further verifying the two-dimensionality of the flow in these regions.

In these same regions, *rms* velocity measurements from the preliminary test matrix show values consistently less than and outside the *rms* velocity range defined by the Z variations of the final test matrix case. Although a specific explanation cannot be offered, these discrepancies are apparently a result of using a cross-film probe with its different flow interferences for data acquisition in the latter experiments. The only other parameter varied between the two sets of data was the airblast atomizer (preliminary measurements used a blank atomizer, i.e., one without a porous plate), but Marakovits[17] showed that the effect of this change on the freestream *rms* velocities is less than 4%.

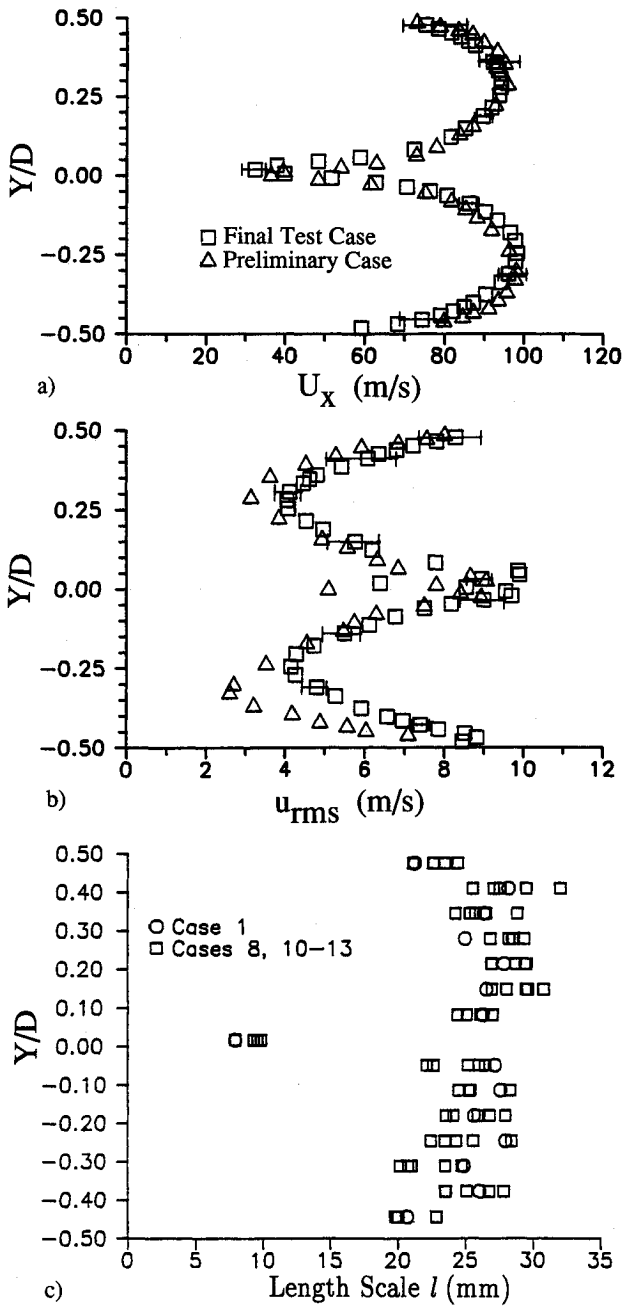

Fig. 11 Comparison of Z-average a) mean and b) *rms* velocity for case 1 of final test matrix with centerline ($Z/D = 0.0$) values for case 1 of preliminary test matrix at $X/D = 0.03$; c) centerline length scale measurements for cases of the final test matrix at $X/D = 0.03$. No liquid injection.

The length scales reported in Fig. 11c are derived by integrating the autocorrelation function and invoking Taylor's hypothesis (for example, see Ref. 24). Freestream scales compare favorably with the largest expected eddy size based on the half-width of the test section minus the splitter plate thickness (33 mm), whereas scales directly downstream of the atomizer tip are on the order of the splitter plate thickness (10.3 mm). Some length scales for cases 7 and 14 were >50 mm. Investigation of the corresponding streamwise autocorrelation functions revealed periodicity at long delay times. These data were thus considered erroneous and eliminated.

The figure shows that case 1 data are typical of those obtained in all cases examined and that length scales are reproducible to order of 10%. Although the averge value for $Y/D < 0$ is slightly less than that for $Y/D > 0$ (27.5 vs 25 mm), both are within a standard deviation of the grand average,

excluding data in the wake, shear layer, and boundary layers. No geometric variations were made during the present experiments; Fig. 11c shows the length scales are independent of air velocity and shear-layer strength. When length scales are altered in work to be performed later, further study of data reduction procedures, including spectral analysis, will be warranted.

One major thrust of this research was to examine the relationship between various local mixing times, defined by Tuttle et al.[14] as

$$\tau_{s\ell,xy} = \ell(X/D,\ Y/D)/u_{rms}(X/D,\ Y/D) \qquad (3)$$

Here ℓ and u_{rms} are both measured at station (X/D, Y/D, $Z/D = 0$).

Figure 12 shows local mixing time normalized with its value at the origin of the shear layer $\tau_{s\ell,00}$ vs Y/D at those axial positions where length scales were measured. Both case 1 and case 14 data reveal that this parameter is essentially similar in the freestream ($Y/D \geq \pm 0.1$), whereas wake or shear-layer values increase with downstream distance. Scatter shown in Fig. 12 appears to result equally from variations in both length scale (Fig. 11c) and *rms* velocity measurements (Fig. 11b). Outside of the wake or shear layer, similarity of $\tau_{s\ell,xy}$ profiles is expected because, except for boundary-layer growth at the Y walls at $Y/D = \pm 0.5$, the length scale, *rms* velocity, and thus local mixing times should not change with X/D. The latter are larger at $Y/D > -0.1$ in case 14 because the nonzero value of λ augments the local mixing time through lower mean (and *rms*) velocities and thus larger mixing or eddy lifetimes.

On or near the tunnel centerline, i.e., within the wake or shear layer, Fig. 13 shows that $\tau_{s\ell,x0}/\tau_{s\ell,00}$ grows linearly in each case. For case 1, from $X/D = 0.03$ to 1.00 length scale increases and *rms* velocity decreases. Downstream the increase in mixing time is primarily due to a decrease in fluctuating velocity. For case 14, eddy size behaves in the same manner as case 1; however, the fluctuating component increases from $X/D = 0.03$ to 1.00 and then decreases. Figure 13 shows that downstream wake or shear-layer mixing times are proportional to $\tau_{s\ell,00}$, which supports the hypothesis of Tuttle et al.[14] that the appropriate time scale is proportional to ℓ/u_{rms}. However, the questions still to be addressed is whether or not the initial mixing time can be related to the global time used in the characteristic time model.

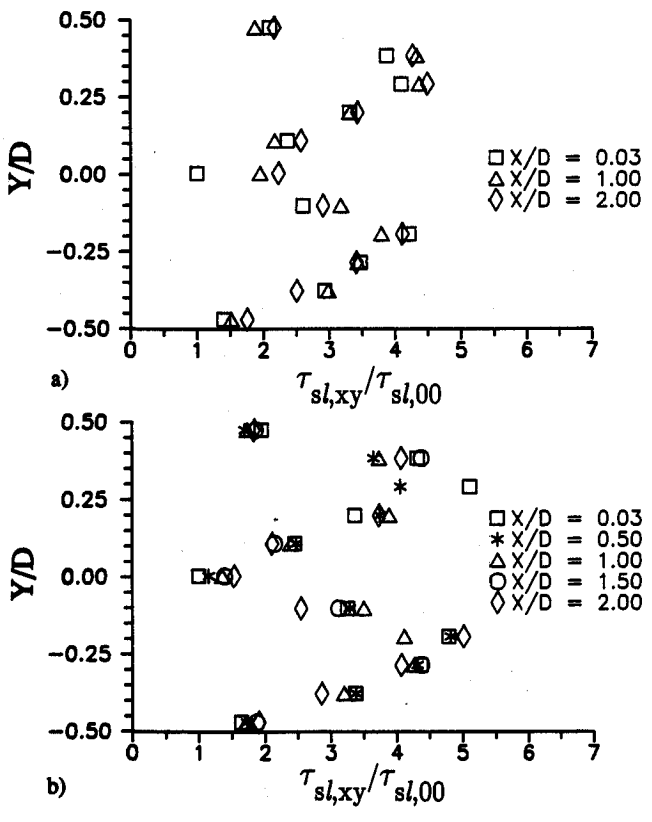

Fig. 12 Experimental centerline ($Z/D = 0.0$) local eddy lifetime profiles for a) case 1 and b) case 14 normalized by the corresponding value of $_{s\ell,00}$ for each case. No liquid injection.

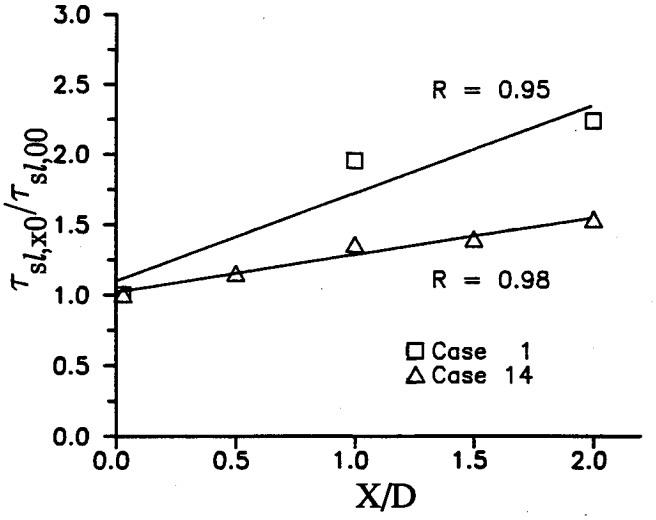

Fig. 13 Experimental local eddy lifetimes at Y/D and $Z/D = 0.0$ normalized by $_{s\ell,00}$ vs axial location. No liquid injection.

The global shear-layer mixing time for a gas turbine combustor is defined in terms of reference velocity and a macroscale of turbulence expressed as a function of primary or secondary air addition hole position and combustor diameter at that location[3]:

$$\ell_{co}^{-1} = (\ell_{\text{pri}} \text{ or } \ell_{\text{sec}})^{-1} + d_{\text{comb}}^{-1} \qquad (4)$$

The dimensions used on the right-hand side of Eq. 4 are shown in Fig. 2. For *CO* emissions, combustion efficiency, and lean blowoff, ℓ_{pri} is usually used in Eq. 4.[4,5,8]

For the origin of the shear layer in the test tunnel, the appropriate macroscale is the atomizer thickness t, and reference velocity is taken as the average of the fuel and air side velocities. From Eq. (2), the latter can be expressed in terms of λ and U_{AFS}, so that

$$\tau_{s\ell,\text{global}} = t(1 + \lambda)/U_{AFS} \qquad (5)$$

where a single velocity and the value of λ have been used to characterize the flow for the tunnel geometry. Figure 14 presents $\tau_{s\ell,00}$ vs $\tau_{s\ell,\text{global}}$ for the eight cases of the final test matrix. Note the linearity of the data for constant values of λ. Also apparent is the decrease in $\tau_{s\ell,00}$ at constant $\tau_{s\ell,\text{global}}$ as shear-layer strength increases, as expected.

Figure 15 recasts the data with the global mixing time in a form more equivalent to its definition for a combustor, a length scale divided by a single velocity characteristic of the complex flow. Thus the x axis in Fig. 15 is relabeled $\tau_{s\ell,co}$ where

$$\tau_{s\ell,co} = t/U_{AFS} \qquad (6)$$

As indicated by the least squares fit given in Fig. 15, the relationship is reasonably accurate considering the small number of data available. However, note that use of U_{AAS} rather than U_{AFS} in Eq. (6) will increase the scatter for a graph analogous to Fig. 15 over that shown in Fig. 14.

Additional experiments are required to explore the effect of variations in length scale on the results presented above.

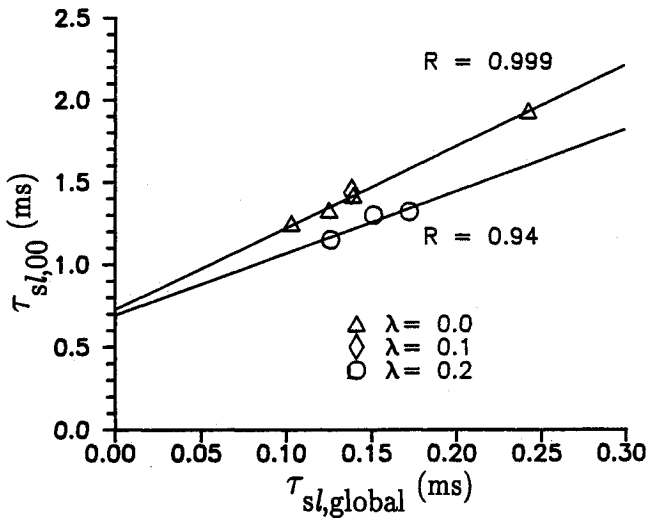

Fig. 14 Comparison of experimental local eddy lifetimes at the shear-layer origin with $\tau_{st,global}$ from the final test matrix. No liquid injection.

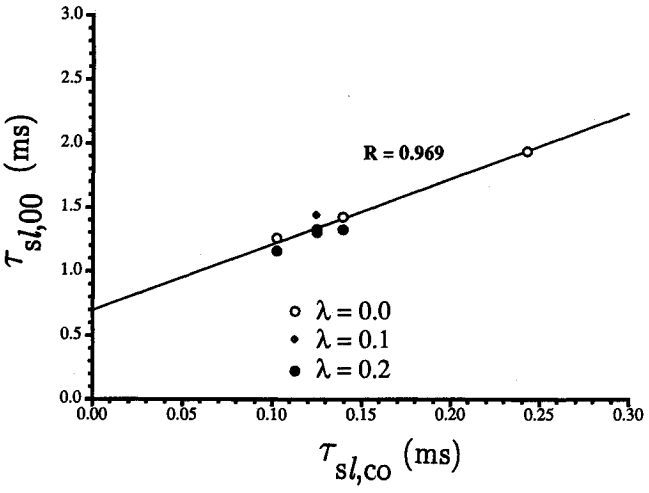

Fig. 15 Comparison of experimental local eddy lifetimes at the shear-layer origin with $\tau_{st,co}$ for the final test matrix. No liquid injection.

Grids and screens upstream of the atomizer tip will vary free-stream scale, as the variation of atomizer thickness is not practical. In the limit of zero thickness, freestream scale is expected to dominate the shear layer: the relationships between these two relevant length scales, as well as atomizer boundary-layer trips and suction, should be explored in further work.

Conclusions

The significance of Fig. 15 is that local mixing times at the origin of the shear layer are proportional to $\tau_{st,co}$ as formulated for a shear layer in Eq. (6), for all eight cases tested in the final test matrix. Coupled with Fig. 13 and 14, the additional conclusion is that $\tau_{st,co}$ does characterize the confined mixing layers studied to date, at least for $X/D \leq 2.0$. Thus the original hypothesis of Tuttle et al.[14] is verified for the region of shear layer growth, which in turn supports the laboratory rig and combustor correlations with $\tau_{st,co}$ for *CO*,[4,14] lean blowoff,[2,8] and combustion efficiency.[5]

The top portion of Fig. 2 represents a primary zone half-section of a typical combustor; for simplicity, no swirler is indicated. A velocity profile showing recirculation and a possible choice for U_{AFS} are also shown. For a given combustor, the shear layer strength is constant because the geometry is fixed. Therefore data for any given combustor should collapse using $\tau_{st,global}$, or $\tau_{st,co}$, as both are proportional to $\tau_{st,00}$.

As shown in Fig. 1, with $\tau_{st,co}$ the characteristic time model collapses data from several combustors on a single curve. Comparison of Fig. 14 and 15 (or defining $\tau_{st,co}$ as t/U_{AAS}) suggests that some of the vertical scatter in the correlations involving $\tau_{st,co}$ is due to using combustor reference velocity[4,5,8] instead of a local velocity in the shear layer surrounding the recirculation zone, which would unfortunately require in situ measurements with combustion in progress.

However, this improved definition for $\tau_{st,co}$ in the primary zone of a turbine combustor could minimize *Y*-axis scatter shown in Fig. 1 and similar correlations for *CO* emissions index[4] and combustion efficiency.[5] Likewise, improved correlations for Sauter mean diameter, with more accurate inclusion of fuel properties and effects of primary zone or swirl-cup airflows, could reduce scatter associated with τ_{eb}, the droplet lifetime. Refined characteristic times for both, which will of necessity include more detailed information than their counterparts used to date, will improve the quality of performance estimates during preliminary analysis of new combustor designs.

Acknowledgments

The work reported here was supported primarily by the Army Research Office under Contract DAAG29-84-K-0165, with Dr. D. M. Mann as technical monitor. David H. Wolf, William H. Frantz, Brian L. Royds, and Prof. David L. Miller assisted in aspects of its experimental portion, which was performed at Drexel University. At Vanderbilt University, Clayton W. Michaels performed analysis on some of the resulting data. We extend our gratitude to all.

References

[1]Zukoski, E. E., and Marble, F. E., "Experiments Concerning the Mechanism of Flame Blowoff from Bluff Bodies," *Proceedings of Gas Dynamics Symposium on Aerothermochemistry*, Northwestern Univ., Evanston, IL, 1956, pp. 205–210.

[2]Plee, S. L., and Mellor, A. M., "Characteristic Time Correlations for Lean Blowoff of Bluff-Body Stabilized Flames," *Combustion and Flame*, Vol. 35, May 1979, pp. 61–80.

[3]Mellor, A. M., "Characteristic Time Emissions Correlations: The T-63 Helicopter Gas Turbine Combustor," *Journal of Energy*, Vol. 1, July-Aug. 1977, pp. 257–262.

[4]Washam, R. M., and Mellor, A. M., "Characteristic Time Correlations of Pollutant Emissions from an Annular Gas Turbine Combustor," *Journal of Energy*, Vol. 3, July-Aug. 1979, pp. 250–253.

[5]Leonard, P. A., and Mellor, A. M., "Correlation of Gas Turbine Combustor Efficiency," *Journal of Energy*, Vol. 7, Nov-Dec. 1983, pp. 596–602.

[6]Leonard, P. A., and Mellor, A. M., "Correlation of Lean Blowoff of Gas Turbine Combustors Using Alternative Fuels," *Journal of Energy*, Vol. 7, Nov.-Dec. 1983, pp. 729–732.

[7]Jarymowycz, T. A., and Mellor, A. M., "Correlation of Lean Blowoff in an Annular Combustor," *Journal of Propulsion and Power*, Vol. 2, March-April 1986, pp. 190–192.

[8]Derr, W. S., and Mellor, A. M., "Characteristic Times for Lean Blowoff in Turbine Combustors," *Journal of Propulsion and Power*, Vol. 3, July-Aug. 1987, pp. 377–380.

[9]Lefebvre, A. H., "Airblast Atomization," *Progress in Energy and Combustion Science*, Vol. 6, No. 3, 1980, pp. 233–261.

[10]Godsave, G. A. E., "Studies of the Combustion of Drops in a Fuel Spray—The Burning of Single Drops of Fuel," *Fourth Symposium (Intl.) on Combustion*, Williams and Wilkins, Baltimore, MD, 1953, pp. 818–830.

[11]Ranz, W. E., and Marshall, W. R., "Evaporation From Drops," *Chemical Engineering Progress*, Vol. 48, April 1952, pp. 173–180.

[12]Kanury, A. M., *Introduction to Combustion Phenomena*, Gordon and Breach, New York, 1975.

[13]Dodge, L. G., "Comparison of Performance of Drop-Sizing Instruments," *Applied Optics*, Vol. 26, April 1987, pp. 1328–1341.

[14]Tuttle, J. H., Colket, M. B., Bilger, R. W., and Mellor, A. M., "Characteristic Times for Combustion and Pollutant Formation in Spray Combustion," *Sixteenth Symposiuim (Intl.) on Combustion*, The Combustion Institute, Pittsburgh, PA, 1977, pp. 209–219.

[15]Rizk, N. K., and Lefebvre, A. H., "Airblast Atomization: Studies on Drop Size Distribution," *Journal of Energy*, Vol. 6, Sept.-Oct. 1982, pp. 323–327.

[16]Tallio, K. V., Prior, R. C., Jr., and Mellor, A. M., "Characteristic Time Model Validation," Army Research Office, Final Report for Contract Number DAAG29-84-K-0165, Research Triangle Park, NC, 1988.

[17]Marakovits, S., "Characterization of a Confined Turbulent Shear Layer," MSME Thesis, Dept. of Mechanical Engineering, Drexel University, Philadelphia, PA, 1987.

[18]Oster, D., and Wyganski, I., "The Forced Mixing Layer Between Parallel Streams," *Journal of Fluid Mechanics*, Vol. 123, Oct. 1982, pp. 91–130.

[19]Brown, G. L., and Roshko, A., "On Density Effects and Large Scale Structure in Turbulent Mixing Layers," *Journal of Fluid Mechanics*, Vol. 64, July 1974, pp. 775–816.

[20]Dobbins, R. A., Crocco, L., and Glassman, I., "Measurement of Mean Particle Size from Diffractively Scattered Light," *AIAA Journal*, Vol. 1, Aug. 1963, pp. 1882–1886.

[21]Rizk, N. K., "Studies on Liquid Sheet Disintegration in Airblast Atomizers," Ph.D. Thesis, School of Mechanical Engineering, Cranfield Institute of Technology, Bedford, UK, 1976.

[22]Sattelmayer, T., and Wittig, S., "Internal Flow Effects in Prefilming Airblast Atomizers: Mechanisms of Atomization and Droplet Spectra," American Society of Mechanical Engineers, New York, ASME Paper 86-GT-150, 1986.

[23]Tallio, K. V., Williamson, J. W., and Mellor, A. M., "Experimental and Numerical Investigation of a Confined Turbulent Shear Flow," Central States Section/The Combustion Institute Spring Technical Meeting, Paper 24, April 30–May 2, Dearborn, MI, 1989.

[24]Tennekes, H., and Lumley, J. L., *A First Course in Turbulence*, MIT Press, Cambridge, MA, 1972.